Beam test of a baseline vertex detector prototype for the CEPC

author list

***Abstract*— The Circular Electron Positron Collide (CEPC) has been proposed to enable more thorough and precise measurements of the properties of Higgs, W and Z bosons, as well as to search for new physics. In response to the stringent performance presented by the vertex detector for the CEPC, we conducted the first test and characterization of a baseline vertex detector prototype using a $6\,\mathrm{GeV}$ electron beam at DESY II Test Beam Line 21. The baseline vertex detector prototype is designed with a cylindrical barrel structure that houses six double-sided ladders. Each side of the ladder includes TaichuPix-3 sensors based on Monolithic Active Pixel Sensor (MAPS) technology, a flex printed cable and a carbon fiber support structure. Additionally, the readout electronics and the Data Acquisition system were verified during this beam test. The performance of the prototype was evaluated using an electron beam that traversed directly the six ladders from one side. Offline data analysis indicates a spatial resolution of about $5\,\mu\mathrm{m}$, with a detection efficiency exceeding $99\,\%$ and an impact parameter resolution also near $5\,\mu\mathrm{m}$. The promising results from this baseline vertex detector prototype mark a significant step toward realizing the optimal vertex detector for the CEPC.**

***Index Terms*— MAPS, Vertex detector, CEPC**

I. Introduction

The CEPC is designed to operate at center-of-mass energies of $91.2\,\mathrm{GeV}$, $160\,\mathrm{GeV}$, and $240\,\mathrm{GeV}$, serving as a Z-boson factory, reaching the threshold for WW pair production, and operating as a Higgs factory, respectively [1]. The abundant production of $b/c-$quark jets during the CEPC operation highlights the critical role of flavor-tagging in the design of the vertex detector. Effective flavor-tagging requires accurate reconstruction of vertex and the trajectory of charged tracks. Therefore, the physics goals of the CEPC are catalyzing the evolution of vertex detector. The vertex detector for CEPC needs to achieve a single-point resolution better than $3\,\mu\mathrm{m}$, maintain a material budget below $0.15\,\%\ X/X_0$ per layer, consume power below $50\,\mathrm{mW\,cm^{-2}}$, and ensure a pixel sensor readout time shorter than $10\,\mu\mathrm{s}$ [1]. In striving to fulfill these requirements, a baseline vertex detector prototype has been designed and tested for the first time using an electron beam provided by DESY II [2].

The research was supported and financed in large part by the National Key Research and Development Program of China under Grant No. 2018YFA0404302 from the Ministry of Science and Technology. Additional support was provided by the Youth Scientist Fund from the National Natural Science Foundation of China under Grant No. 12205313." *xxxxx*

The next few paragraphs should contain the authors' current affiliations, including current address and e-mail. For example, F. A. Author is with the National Institute of Standards and Technology, Boulder, CO 80305 USA (e-mail: author@boulder.nist.gov).

S. B. Author, Jr., was with Rice University, Houston, TX 77005 USA. He is now with the Department of Physics, Colorado State University, Fort Collins, CO 80523 USA (e-mail: author@lamar.colostate.edu).

T. C. Author is with the Electrical Engineering Department, University of Colorado, Boulder, CO 80309 USA, on leave from the National Research Institute for Metals, Tsukuba, Japan (e-mail: author@nrim.go.jp).

The baseline vertex detector prototype comprises three layers of concentric barrels positioned at radii rangeing from $18.7\,\mathrm{mm}$ to $60.5\,\mathrm{mm}$. The mechanical structure of the baseline vertex detector is fabricated according to the design proposed in the CEPC conceptual design report, and is built to full scale [1]. The detector module, also known as the ladder, is a double-sided structure, consisting of CMOS Monolithic Active Pixel Sensors (MAPS), with up to ten on each side, flex print cables (FPCs), and a support structure made of carbon fiber as depicted in Fig. 1 (a). Two sensors are wire-bonded onto the end of the FPC to cover the maximum area allowed by the collimator, which measures $2.5\,\mathrm{cm} \times 2.5\,\mathrm{cm}$. Control, power and data transfer is provided to the sensor by the FPCs. The ladder has a thickness of approximately $3.67\,\mathrm{mm}$ and a length of about $553\,\mathrm{mm}$. Six ladders are mounted along a certain diameter direction of the concentric barrels, as shown in Fig. 1 (b).

The prototype is based on the MAPS TaichuPix-3, produced with a $180\,\mathrm{nm}$ CMOS Imaging Sensor (CIS) technology [3], [4], [5]. The TaichuPix-3 has a dimension of $2.57\,\mathrm{cm} \times 1.59\,\mathrm{cm}$ and contain 1024 columns $\times$ 512 rows with a pixel pitch of $25\,\mu\mathrm{m} \times 25\,\mu\mathrm{m}$. The TaichuPix-3 is based on a column drain readout architecture with binary encoded data output. The power consumption of TaichuPix-3 is less than $200\,\mathrm{mW\,cm^{-2}}$ when operating at a fast leading edge ($< 200\,\mathrm{ns}$) of the analog front-end and a serializer interface of $160\,\mathrm{MHz}$. The TaichuPix-3 is characterized by the utilization of two different processes, namely Process A and Process B. Process A is fabricated using the standard back-bias diode process and includes an extra deep N-layer mask compared to Process B, as detailed in [6]. The performance of TaichuPix-3 sensors have been verified under a $4\,\mathrm{GeV}$ electron beam at DESY II, including the intrinsic spatial resolution of $4.8\,\mu\mathrm{m}$ for Process A and $4.5\,\mu\mathrm{m}$ for Process B, with a detection efficiency exceeding $99\,\%$, as reported in [7]. In total, 24 TaichuPix-3 sensors with thickness of $150\,\mu\mathrm{m}$ were assembled to the prototype.

In order to evaluate the performance of the mechanical, electrical, Data Acquisition system (DAQ) of the baseline vertex detector, a beam test was conducted in April 2023 at the DESY II Test Beam Line 21 (TB 21) [2]. The electron beam

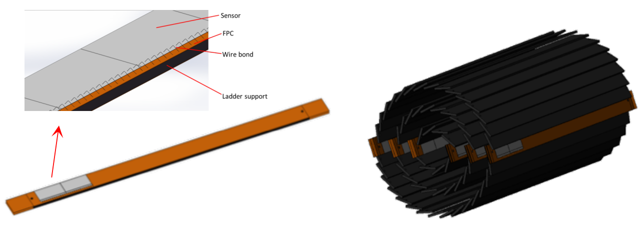

(a) (b)

Fig. 1. (a) detector module, also known as ladder; (b) Structure of the baseline vertex detector prototype [8].

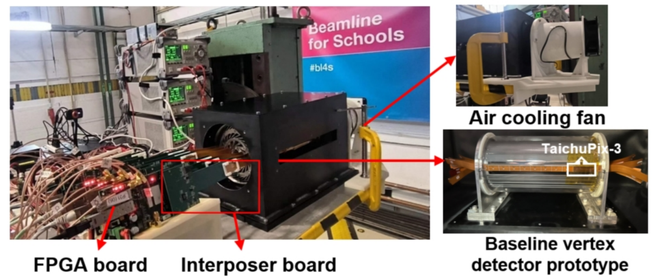

Fig. 2. Baseline vertex detector prototype setup at DESY II TB21.

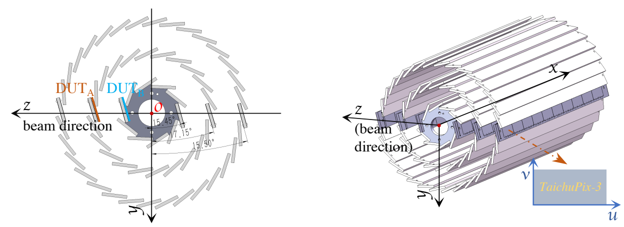

(a) (b)

Fig. 3. (a) shows the position of $\mathrm{DUT}_{\boldsymbol{A}}$ in blue color and $\mathrm{DUT}_{\boldsymbol{B}}$ in yellow color, as well as the definition of the global coordinate system. z-direction is the electron beam direction. (b) shows the definition of the local coordinate system on each TaichuPix-3 chip, where the u-direction runs along the row direction of the chip, and the v-direction runs along the column direction of the chip.

was directed through the six ladders installed on the prototype, generating precise reconstruction points using the multi-layer TaichuPix-3 sensors. In this paper, the test beam setup are described in detail, and the characterization of the baseline vertex prototype obtained from the offline data analysis are reported and discussed.

II. Test beam setup

The experimental setup is depicted in Fig. 2. The prototype is placed within a black box, which includes an opening on the side where the ladders are installed, enabling the beam to directly hit the ladders. The readout module of each ladder consists of an interposer board, an FPGA readout board, and a SiTCP protocol Ethernet port, as depicted in Fig. 2. The interposer board is used to transmit data from fired pixels and control signals between the ladder and the FPGA readout board, also supplies DC voltages to the ladders. Each FPGA is enabled and synchronizes the clock through three synchronous ports: the clock controller port, global configuration port, and timestamp synchronization port. The data package is transmitted through the Ethernet port to the switch and subsequently sent to the host computer. A dedicated DAQ system has been developed for the data collection. The DAQ system also includes an interface for real-time sampling output, which is used to monitor the beam status.

During the beam test, the readout system operated reliably throughout all production run and the recorded maximum data rate was about $18\ \mathrm{MB{\cdot}s^{-1}}$. An electric fan was used to utilized to cool the prototype as depicted in Fig. 2, effectively reducing the temperature of the outermost layer from $40\,^{\circ}\mathrm{C}$ to $28\,^{\circ}\mathrm{C}$, as measured with an infrared camera.

The analysis of the offline data is based on TaichuPix-3 sensors with Process A and Process B, which are positioned as shown in Fig. 3(a), and labeled as DUT_A and DUT_B, respectively. When one DUT is under study, the other planes are used to determine the reference tracks. The TaichuPix-3 sensors are operated in a trigger-less mode. An example of hitmap is depicted in Fig. 4, demonstrating the proper functioning of the entire detection system.

III. Offline analysis and results

The offline analysis procedure consists of several steps, including decoding raw data, clustering, track finding and reconstruction, alignment of the detector geometry. Specifically, clustering is the process of grouping adjacent pixels with the collected charge above the set threshold, and the center of the cluster is calculated using the the Center of Gravity (CoG) method. The tracks are reconstructed using the General Broken Line (GBL) package [9], which accounts for multiple scatter effects. The geometry of the prototype is aligned using the Millepede algorithm [10], with the alignment parameters consisting of three translations and three rotations for each sensor. These alignment parameters are determined by minimizing the residual predicted by the track model, which is related to the track parameters and alignment parameters.

The threshold is a crucial parameter for evaluating the detector performance, and a threshold scan was performed during the beam test. As discussed in Ref. [5], the pixel biasing is achieved through the integrated DAC on the periphery. The threshold of the pixel increases with the biasing parameter ‘ITHR’ controlled by an 8-bit DAC code. When the other biasing parameters remain constant, a larger DAC code of ITHR leads to a higher threshold.

A. Cluster Size

The cluster size is the number of neighboring fired pixels with signals above a certain threshold. A higher threshold leads to a reduction in fired pixels, consequently weakening the charge-sharing effect and resulting in a deterioration in spatial resolution. As depicted in Fig. 5, the average cluster size for DUT_A and DUT_B is shown as a function of threshold. It is observed that the cluster size decreases as the threshold increases. At the minimum threshold, the averaged cluster

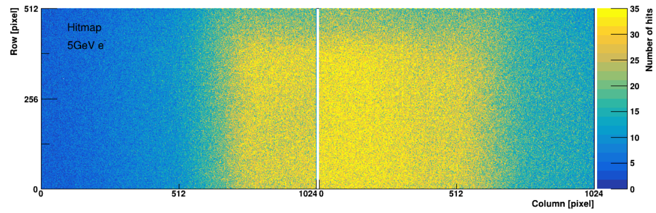

Fig. 4. The hitmap under 5 GeV electron beam.

size for DUT$_A$ and DUT$_B$ is 1.74 pixels and 2.65 pixels, respectively. Furthermore, the cluster size of DUT$_A$ is smaller than that of DUT$_B$, indicating a reduced charge-sharing effect in DUT$_A$. This difference is attributed to the additional deep N-layer mask in DUT$_A$, as demonstrated in [6].

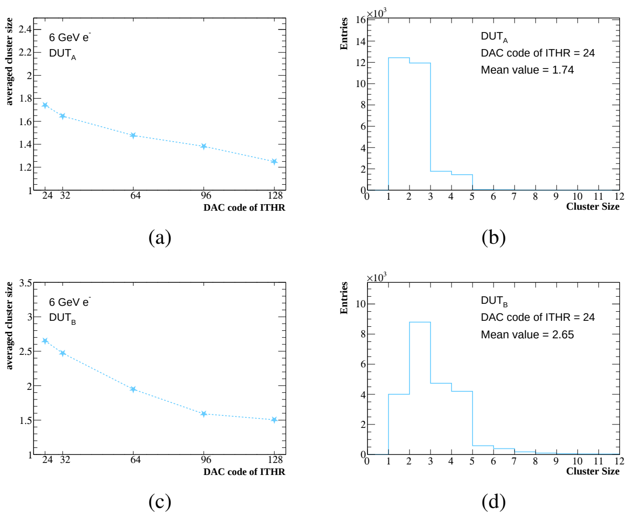

Fig. 5. (a) and (c) show the variation of cluster size with threshold for DUT$_A$ and DUT$_B$, respectively. The cluster size distribution of DUT$_A$ and DUT$_B$ at the lowest threshold are displayed in (b) (d).

B. Spatial resolution

The spatial resolution is derived from an unbiased residual distribution using the GBL algorithm for track fitting which exclude the DUT. The scattering angle is predicted using the Highland formula [9]. Following alignment, the difference between the predicted and measured hit positions on the DUT is shown in Fig. 6 and is fitted using a Gaussian function. The standard deviation for DUT$_B$ at a threshold of 24 is approximately 5 µm. Additionally, as depicted in Fig. 7 (a), the spatial resolution of both DUTs deteriorates as the threshold increases, and due to reduced charge-sharing effects on DUT$_A$, it exhibits poorer resolution compared to DUT$_B$. At the lowest setting threshold, the best spatial resolution achieved is 5.38 µm in the u-direction and 5.52 µm in the v-direction for DUT$_A$, and 4.97 µm in the u-direction and 5.21 µm in the v-direction for DUT$_B$.

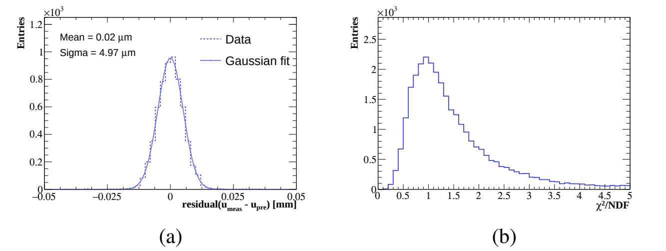

Fig. 6. (a) The unbiased residual distribution is shown in $\boldsymbol{u}$-direction at threshold of 24, using DUT$_{\boldsymbol{B}}$ as an example. (b) Distribution of the $\boldsymbol{\chi^2}$ per degree of freedom

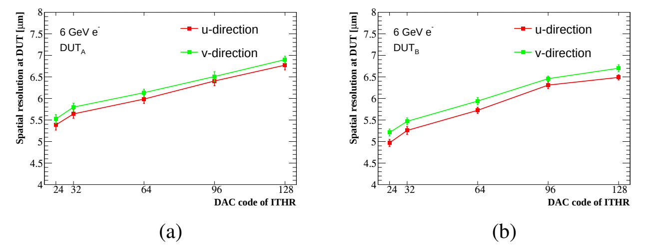

Fig. 7. The variation of spatial resolution with threshold for DUT$_{\boldsymbol{A}}$ and DUT$_{\boldsymbol{B}}$. The error bars represent the systematic uncertainty from the beam energy spread (5%) [9] and a accuracy of the scattering angle predicted by Highland formula (11%) [2]. The statistical error is small enough to be negligible.

C. Detection efficiency

The detection efficiency is defined as the ratio of the number of tracks that can match the measured points on the DUT ($N^{tracks}_{matched}$) to the total number of tracks (N^{tracks}_{all}). The selection of matched tracks is based on whether the difference between the extrapolated hit positions of the tracks on the DUT and the measured hit positions on the DUT is within a specified distance d. In this analysis, d is set to 100 µm to exclude poorly reconstructed tracks. The detection efficiency can be expressed as follows:

$$Eff. = \frac{N^{matched\ tracks}_{|x_{meas},y_{meas}-x_{pre},y_{pre}|<d}}{N^{tracks}_{all}} \tag{1}$$

As shown in Fig. 8, the efficiency of DUT$_A$ and DUT$_B$ exhibit a decreasing trend as the threshold increases. The maximum detection efficiency is 99.4 % and 99.6 % for DUT$_A$ and DUT$_B$, respectively.

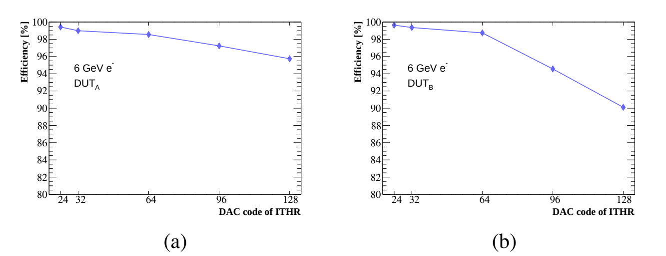

Fig. 8. The detection efficiency of DUT$_{\boldsymbol{mod}}$ and DUT$_{\boldsymbol{std}}$ as a function of the threshold setting ‘ITHR’.

D. Impact parameters

The impact parameter is defined as the perpendicular distance between the track and the primary vertex. In the case of this beam test, the electron beam directly passed through six ladders from one side of the vertex detector prototype. Each electron track is split into an upstream track and a downstream track, based on hit points from the first three ladder layers and the last three ladder layers, respectively. The upstream track and downstream track are fitted separately. A loose track quality cut, with $\chi 2/N_{DoF} < 3$, is applied. As depicted in Fig. 9 (a), the primary vertex (x_{pv}, y_{pv}) is assumed to be the midpoint between the two points (x_{up}, y_{up}) and (x_{dn}, y_{dn}), where the upstream and downstream tracks extrapolated to the $z = 0$ plane. In Fig. 9 (b) the impact parameter is calculated as the perpendicular distance from the primary vertex (x_{pv}, y_{pv}) to either the upstream or downstream track. Even though the impact parameter is not strictly well-defined, it can still reflect the overall performance of the vertex detector prototype.

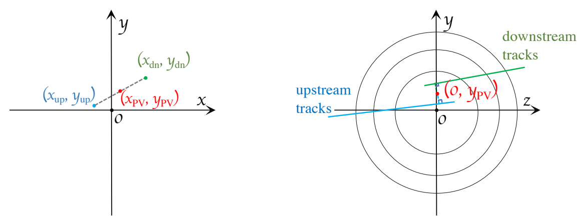

(a) (b)

Fig. 9. (a) (x_{up}, y_{up}) and (x_{dn}, y_{dn}) represent the extrapolated positions of upstream track and downstream track at $z = 0$ plane. The point (x_{pv}, y_{pv}) denotes the midpoint between (x_{up}, y_{up}) and (x_{dn}, y_{dn}). (b) taking $y-z$ plane as an example, the impact parameter is the perpendicular distance to the tracks.

Therefore, Fig. 10 shows the perpendicular distances of the primary vertex and the upstream track in $x - z$ plane and $y - z$ plane, with a resolution of $5.06\,\mu\text{m}$ in the x-direction and $5.14\,\mu\text{m}$ in the y-direction for the impact parameter.

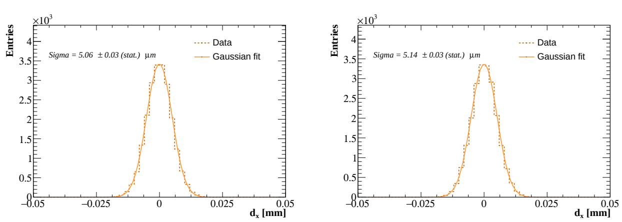

(a) (b)

Fig. 10. The distribution of distance between upstream tracks and PV at $x - z$ plane (a) and $y - z$ plane (b).

IV. Conclusion

A first baseline vertex detector prototype developed for CEPC has been tested and characterized using a 6 GeV electron beam at DESY II TB 21. Six ladders with 24 TaichuPix-3 sensors were installed onto the mechanical structure of the prototype. The electronics and the DAQ system have been tested, and remained stable during beam test. The offline analysis results show good performance of the prototype, with a spatial resolution of about $5\,\mu\text{m}$ for TaichuPix-3 chips with Process B at the innermost ladder and $5.4\,\mu\text{m}$ for TaichuPix-3 chips with Process A at the middle layer ladder. The detection efficiency of about 99% has been obtained for the prototype. The resolution of impact parameter is about $5.1\,\mu\text{m}$ when assuming the collision point at the $z = 0$ plane.

Acknowledgment

The measurements leading to these results have been performed at the Test Beam Facility at DESY Hamburg (Germany), a member of the Helmholtz Association (HGF).

References

[1] The CEPC Study Group, "CEPC Conceptual Design Report: Volume 2 - Physics & Detector," 11 2018.

[2] R. Diener, J. Dreyling-Eschweiler, H. Ehrlichmann, I. Gregor, U. Kötz, U. Krämer, N. Meyners, N. Potylitsina-Kube, A. Schütz, P. Schütze, and M. Stanitzki, "The DESY II test beam facility," *Nucl. Instrum. Meth. A*, vol. 922, pp. 265–286, 2019.

[3] X. Wei *et al.*, "High data-rate readout logic design of a 512 × 1024 pixel array dedicated for CEPC vertex detector," *JINST*, vol. 14, no. 12, p. C12012, 2019.

[4] T. Wu *et al.*, "The TaichuPix1: a monolithic active pixel sensor with fast in-pixel readout electronics for the CEPC vertex detector," *JINST*, vol. 16, no. 09, p. P09020, 2021.

[5] Y. Zhang *et al.*, "Development of a CMOS pixel sensor prototype for the high hit rate CEPC vertex detector," *Nucl. Instrum. Meth. A*, vol. 1042, p. 167442, 2022.

[6] W. Snoeys *et al.*, "A process modification for CMOS monolithic active pixel sensors for enhanced depletion, timing performance and radiation tolerance," *Nucl. Instrum. Meth. A*, vol. 871, pp. 90–96, 2017.

[7] T. Wu, S. Li, W. Wang *et al.*, "Beam test of a 180nm cmos pixel sensor for the cepc vertex detector," *Nuclear Instruments and Methods in Physics Research Section A: Accelerators, Spectrometers, Detectors and Associated Equipment*, vol. 1059, p. 168945, 2024.

[8] J. Fu, Z. Liang, H. Zeng, G. Li, M.-M. Dong, H. min Qu, and J. B. G. da Costa, "Mechanical design of an ultra-light vertex detector prototype for cepc," *Radiation Detection Technology and Methods*, vol. 6, pp. 159 – 169, 2022. [Online]. Available: https://api.semanticscholar.org/CorpusID:257090845

[9] C. Kleinwort, "General broken lines as advanced track fitting method," *Nuclear Instruments and Methods in Physics Research Section A: Accelerators, Spectrometers, Detectors and Associated Equipment*, vol. 673, pp. 107–110, 2012. [Online]. Available: https://www.sciencedirect.com/science/article/pii/S0168900212000642

[10] V. Blobel, "Software alignment for tracking detectors," *Nuclear Instruments and Methods in Physics Research Section A: Accelerators, Spectrometers, Detectors and Associated Equipment*, vol. 566, no. 1, pp. 5–13, 2006, tIME 2005. [Online]. Available: https://www.sciencedirect.com/science/article/pii/S0168900206007984